Acta Crystallographica Section D
Biological Crystallography
ISSN 0907-4449

Unusual space-group pseudosymmetry in crystals of human phosphopantothenoylcysteine decarboxylase

Narayanan Manoj and Steven E. Ealick*

Department of Chemistry and Chemical Biology, Cornell University, Ithaca, NY 14853, USA

Correspondence e-mail: see3@cornell.edu

Received 27 June 2003
Accepted 22 July 2003

PDB Reference:
phosphopantothenoylcysteine decarboxylase, 1qzu, r1qzusf.

Phosphopantothenoylcysteine (PPC) decarboxylase is an essential enzyme in the biosynthesis of coenzyme A and catalyzes the decarboxylation of PPC to phosphopantetheine. Human PPC decarboxylase has been expressed in *Escherichia coli*, purified and crystallized. The Laue class of the diffraction data appears to be $\bar{3}m$, suggesting space group $R32$ with two monomers per asymmetric unit. However, the crystals belong to the space group $R3$ and the asymmetric unit contains four monomers. The structure has been solved using molecular replacement and refined to a current R factor of 29%. The crystal packing can be considered as two interlaced lattices, each consistent with space group $R32$ and with the corresponding twofold axes parallel to each other but separated along the threefold axis. Thus, the true space group is $R3$ with four monomers per asymmetric unit.

1. Introduction

Coenzyme A and phosphopantetheine function as acyl carriers and carbonyl-activating groups in a number of biochemical reactions and are essential cofactors in all living cells. These cofactors play a key role in the biosynthesis and breakdown of fatty acids, in the biosynthesis of nonribosomal peptides and polyketides and in many other biochemical pathways. The biosynthesis of coenzyme A from pantothenate (vitamin B_5) contains five universal steps (Begley *et al.*, 2001). Phosphopantothenoylcysteine (PPC) synthetase, the second enzyme in this pathway, catalyzes the formation of PPC from 4′-phosphopantothenate and cysteine. Phosphopantothenoylcysteine decarboxylase, the next enzyme in the pathway, catalyzes the decarboxylation of PPC to form 4′-phosphopantetheine. This reaction is carried out as an FMN-dependent redox reaction (Daugherty *et al.*, 2002; Hernandez-Acosta *et al.*, 2002; Kupke, 2001; Kupke *et al.*, 2001; Strauss & Begley, 2001). In humans, PPC synthetase and PPC decarboxylase are encoded by separate genes *coaB* and *coaC*, respectively, while in some prokaryotes (*e.g. Escherichia coli*) these genes are fused, where the N-terminal domain of the protein catalyzes the decarboxylation of PPC.

The crystal structures of the *Arabidopsis thaliana* PPC decarboxylase AtHAL3a and its mutant complexed with a substrate intermediate are known (Albert *et al.*, 2000; Steinbacher *et al.*, 2003). AtHAL3a is a homotrimeric α/β protein. Each subunit consists of a six-stranded parallel β-sheet sandwiched between two layers of α-helices and the fold corresponds to an NAD(P)-binding Rossmann-fold domain. The structure of the complex revealed aspects of the enzyme interactions relevant to the catalysis.

We have initiated structural studies on the human PPC decarboxylase and its complexes with product and substrate analogs in order to elucidate differences between the human and plant enzymes and to understand how the enzyme stabilizes high-energy carbanions. The human PPC decarboxylase is a 22.4 kDa protein of 204 amino acids and is 50% identical and 63% similar to the *A. thaliana* PPC decarboxylase. Here, we report the purification, crystallization and initial structure determination of human PPC decarboxylase.

The structure determination was complicated by the presence of pseudosymmetry. The paper also addresses the characterization of pseudosymmetry in the crystal form and the identification of the true space group.

2. Materials and methods

2.1. Protein expression and purification

The human *coaC* gene was cloned into a pPROEX-HTa (Invitrogen) vector containing the *trp* promoter, a six-histidine tag and a tobacco etch virus (TEV) protease cleavage site and transformed into *E. coli* strain B834(DE3) (Novagen) as described previously (Daugherty *et al.*, 2002). The native protein was obtained by inoculating 1 l of LB and 100 µg ml^{-1} ampicillin with 5 ml of a saturated starter culture. The cells were grown at 310 K until they reached an OD_{600} of ∼0.6 and were induced with 800 µ*M* isopropyl-β-D-thiogalactoside. The cells were harvested after 4 h by centrifugation at 5000*g* for 10 min and stored at 193 K.

All purification steps were carried out at 277 K. Cells were resuspended in 20 ml of wash buffer (50 m*M* Tris–HCl, 500 m*M* NaCl and 20 m*M* imidazole pH 8.0) and broken using a French press. The crude extract was centrifuged and the resulting supernatant was mixed for 1 h with 2 ml Ni–NTA resin (Novagen) equilibrated with wash buffer. The resin was added to a polypropylene column and washed with 200 ml of wash buffer. PPC decarboxylase was then eluted from the column using wash buffer containing 200 m*M* imidazole. The protein was then buffer-exchanged into 10 m*M* Tris–HCl pH 8.0 by dialysis and concentrated to ∼10 mg ml^{-1} (sample *A*). In order to remove the polyhistidine tag, the protein was incubated with TEV protease (Invitrogen) for ∼24 h at 277 K. The protein mixture was then buffer-exchanged into the initial wash buffer and mixed with 500 µl of Ni–NTA resin and added to a polypropylene column. The purified PPC decarboxylase in the flowthrough was buffer-exchanged into storage buffer (10 m*M* Tris–HCl pH 8.0) and concentrated to ∼9 mg ml^{-1} (sample *B*).

2.2. Crystallization and data collection

Crystallization trials were performed on both protein samples *A* and *B*. Initial crystallization conditions for sample *B* were identified from trials using Crystal Screen II (Hampton Research). Crystals of PPC decarboxylase were grown using the hanging-drop method with each drop containing 1 µl of 8 mg ml^{-1} protein, 4 m*M* of phosphopantetheine and 1 µl of reservoir solution equilibrated against a reservoir volume of 0.5 ml. The optimized reservoir solution contained 1.5 *M* $(NH_4)_2SO_4$, 100 m*M* MES pH 5.4 and 10% dioxane. The best crystals grew to a maximum size of 0.12 × 0.12 × 0.05 mm in about 15 d.

Table 1
Summary of data-collection and processing statistics.

Values for the outer resolution shell (3.0–2.9 Å) are given in parentheses.

Resolution (Å)	30–2.9	30–2.9
Space group	*R*32	*R*3
Unit-cell parameters (Å)	a = 124.8, c = 153.5	a = 124.8, c = 153.5
No. of reflections	43233	43418
No. of unique reflections	9890	18689
Redundancy	4.4 (4.4)	2.3 (2.3)
Completeness (%)	97.0 (98.8)	96.2 (98.3)
Mean $I/\sigma(I)$	30.7 (4.7)	22.6 (3.4)
Linear $R_{\rm merge}$† (%)	5.0 (32.1)	4.5 (28.1)
Square $R_{\rm merge}$‡ (%)	3.6 (25.7)	3.2 (22.8)
χ^2§	1.7 (1.0)	1.7 (1.0)

† $R_{\rm merge} = \sum_{hkl}\sum_i |I_{hkli} - \langle I_{hkl}\rangle|/\sum N_{hkl}\langle I_{hkl}\rangle$. ‡ $R_{\rm merge} = \sum_{hkl}\sum_i (I_{hkli} - \langle I_{hkl}\rangle)^2/\sum N_{hkl}\langle I_{hkl}\rangle^2$. § $\chi = \sum_{hkl}\sum_i (I_{hkli} - \langle I_{hkl}\rangle)^2/[\sigma^2(I)N_{hkl}(N_{hkl}-1)]$.

Monochromatic X-ray intensity data were measured at beamline 8-BM at the Advanced Photon Source using a Quantum 315 detector (Area Detector Systems Corporation). Prior to flash-freezing, the crystals were transferred to a cryoprotectant solution similar to the mother liquor but containing 12% ethylene glycol. The crystals were then frozen directly in liquid nitrogen. Data from the crystal were collected over a range of 75° using a 0.5° oscillation step with a crystal-to-detector distance of 300 mm. The *HKL* suite of programs was used for integration and scaling of the data (Otwinowski & Minor, 1997).

3. Results and discussion

3.1. Determination of correct space group

The crystal unit-cell parameters show nearly cubic morphology; in fact, the diffraction images could be easily indexed and processed in a primitive cubic lattice with unit-cell parameter a = 88 Å, but efforts to merge the data set with either cubic Laue symmetry were unsuccessful. The next acceptable lattice was a rhombohedral lattice with approximate unit-cell parameters a = 124, c = 154 Å. The data set could be processed and merged in space group *R*32 to an $R_{\rm merge}$ value of ∼12% and a data completeness of ∼90%, but with about 45% of the measured reflections being rejected as outliers. The large number of outliers in the merged data set is the consequence of a wrong choice of the order of axes assigned by autoindexing owing to the pseudo-cubic cell dimensions. Although there are three body diagonals in the pseudo-cubic unit cell, only one of them is a threefold axis in a rhombohedral space group. The data set was finally indexed and integrated in the triclinic space group and subsequently reindexed and merged in space group *R*32 using the choice of axes that resulted in the lowest $R_{\rm merge}$ value and minimum number of rejected outliers. Assuming two molecules in the asymmetric unit, the crystal has a $V_{\rm M}$ of 2.5 Å^3 Da^{-1}

(Matthews, 1968). The statistics of this data set are given in Table 1.

Molecular-replacement calculations were performed using the program *AMoRe* (Navaza & Saludjian, 1997) using a monomer from the structure of the plant PPC decarboxylase (PDB code 1e20; Albert *et al.*, 2000) as the search model. The search model used contained all the conserved residues between the plant and human enzymes, while the dissimilar residues were mutated to alanine residues and no FMN was included. Unambiguous solutions for two monomers in the asymmetric unit were obtained using reflections in the resolution range 15.0–3.0 Å (Table 2). The best solution had a correlation coefficient (CC) of 0.486 and an *R* factor of 0.48. The next best solution had a CC of 0.305 and an *R* factor of 0.543. A translational pseudosymmetry between the two monomers was indicated by a large peak in the self-Patterson (35% of that of the origin peak) at about (0, 0, 1/2). An analysis of the crystal packing showed that the axes of symmetry of the two trimers coincide with the crystallographic threefold rotation axis. Along the threefold axis, the trimers adopt two orientations corresponding to 0 and 180° rotation perpendicular to the threefold. These orientations alternate along the *c* axis such that the molecules pack face to face along the threefold axis (Fig. 1). The packing also revealed short contacts in the region of residues 71–87 among the twofold-related molecules at alternate positions along the *c* axis.

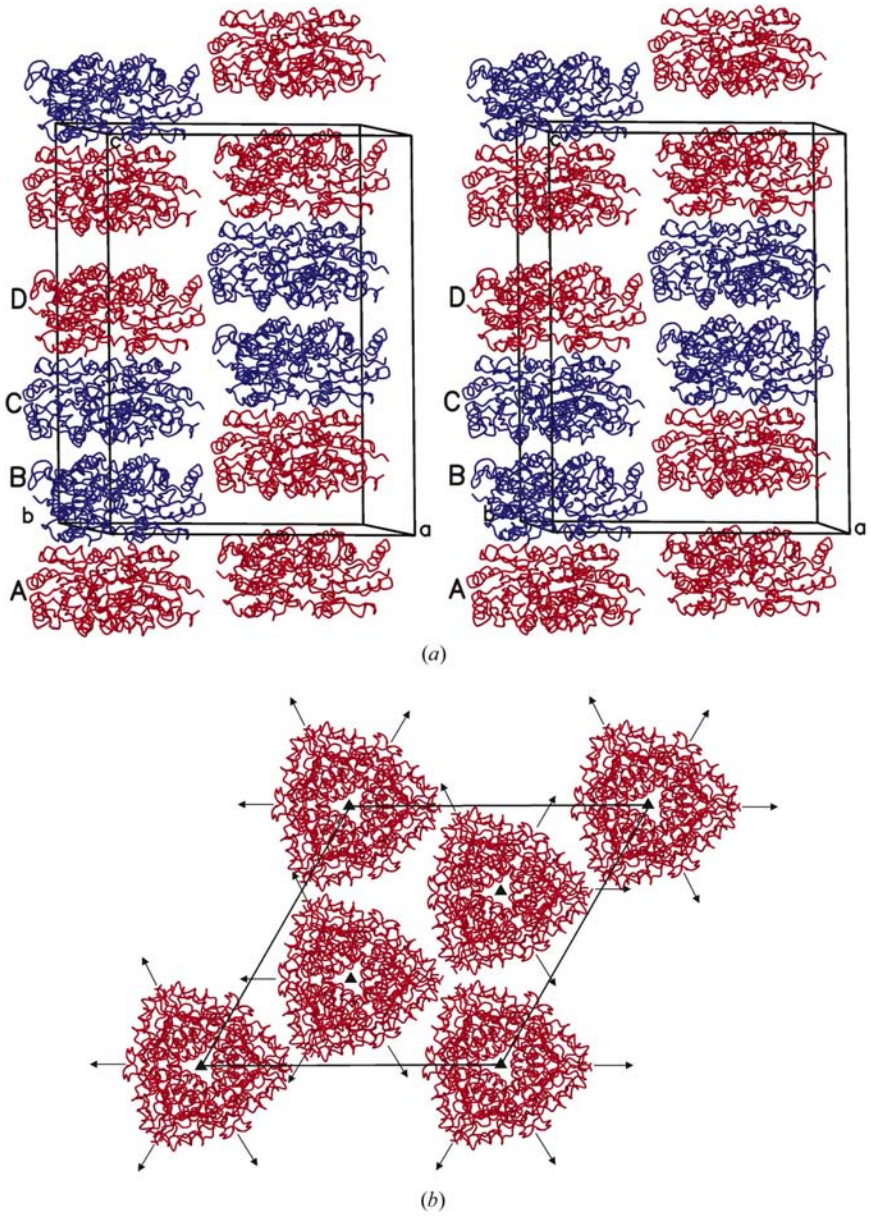

Figure 1
Packing arrangement in *R*3. (*a*) View perpendicular to the *c* axis. The red molecules and the blue molecules form two independent crystal patterns with *R*32 symmetry. However, the twofold axis relating the red molecules is shifted by about 4.0 Å along the vertical direction (*c* axis) from the twofold axis relating the blue molecules. (*b*) View down the *c* axis. The two twofold axes for the red trimers and blue trimers are parallel to each other and perpendicular to the *c* axis. Owing to the 4.0 Å shift, the twofold symmetry of the entire crystal structure is thus lost. This figure was created using *MOLSCRIPT* (Kraulis, 1991) and *RASTER3D* (Merritt & Bacon, 1997).

Refinement of the model using the program *CNS* (Brünger *et al.*, 1998) did not improve the model, as reflected in the high free-*R* and *R* values (*R* value > 45%), and one of the monomers had very poor electron density. Analysis of cumulative intensity distributions and moments did not indicate the presence of twinning. For acentric untwinned data the expected ratio of the average square intensity to the square of the average intensities ($\langle I^2\rangle/\langle I\rangle^2$) is 2, while for perfectly twinned data it is 1.5. For the *R*32 data set the value was 2.7. The values of the moments of *I* all lie above the theoretical values because of the translational pseudosymmetry. The different nature of the packing interactions around the alternating twofold axes along the *c* axis pointed to a space group in which the twofold symmetry is obeyed by only half the molecules in the unit cell, giving rise to lower symmetry with *R*3 packing.

3.2. Structure solution, refinement and crystal packing in space group *R*3

Subsequently, the intensity data were processed again in space group *R*3 (Table 1). The structure solution was obtained for space group *R*3 using *AMoRe*. Unambiguous solutions for four monomers were obtained using one monomer of AtHAL3a as the search model and using data in the resolution range 15.0–3.0 Å (Table 2). The values obtained for the CC and *R* factor for the best solution were 0.604 and 0.467, respectively. The next best solution had a CC of 0.567 and an *R* factor of 0.491. The

Table 2
Molecular-replacement data.

α, β and γ are Eulerian angles and T_x, T_y and T_z are fractional Cartesian coordinates. CC is the correlation coefficient.

(*a*) Space group *R*32.

	α (°)	β (°)	γ (°)	T_x	T_y	T_z	CC	*R* factor
(1)	39.6	30.5	369.2	0.2828	0.7850	0.2831	26.6	55.3
(2)	42.6	31.5	368.5	0.6110	0.4463	0.4235	48.6	48.2

(*b*) Space group *R*3.

	α (°)	β (°)	γ (°)	T_x	T_y	T_z	CC	*R* factor
(1)	78.0	151.2	188.0	0.7830	0.2821	0.0006	37.6	56.1
(2)	77.0	149.8	188.8	0.1125	0.9438	0.1930	53.6	52.6
(3)	42.2	30.9	9.6	0.6103	0.4460	0.2322	55.3	49.1
(4)	37.0	29.3	11.1	0.2861	0.7864	0.0932	60.4	46.7

crystal packing revealed no short contacts and electron-density maps showed that the four monomers were well ordered and the FMN that had been omitted from the search model was clear in each monomer (Fig. 2). The structure was refined using *CNS* and the program *O* (Jones *et al.*, 1991) was used for model building. Non-crystallographic symmetry constraints and restraints as implemented in *CNS* were used throughout the refinement and the conventional and free *R* factors are 0.295 and 0.339, respectively.

Each of the four monomers in the asymmetric unit is related to two of the others by a pseudo-twofold rotation about the face diagonal $a + b$ followed by a translation along the *c* axis and is related to the third monomer by a pure translation along the *c* axis. The crystal packing can be described as two almost independent *R*32 crystal patterns that are interlaced. The twofold axes corresponding to the two patterns are perpendicular to *c* and parallel to each other. However, the twofold axes of the individual patterns are separated by a significant shift of 4.0 Å along the *c* axis, which results in the loss of twofold symmetry for the entire crystal and thus gives rise to *R*3 symmetry (Fig. 1). Initial packing analysis showed that there were no crystal contacts between C^{α} atoms of less than 5 Å, either between the two crystal patterns or between the independent trimers within each crystal pattern.

Three kinds of crystal-packing interaction are observed in the refined structure. A total of 2500 Å^2 of surface area is buried between the *A* trimer and the *B* trimer. Each monomer *A* and *B* contributes six residues with crystal contacts less than 3.6 Å. A total of 2135 Å^2 of surface area is buried between the *C* trimer and the *D* trimer. Each monomer *C* and *D* contributes five residues with contacts less than 3.6 Å. The *AB* and *CD* trimer pairs form columns parallel to the *c* axis. The columns are linked by the C-terminal helix of each monomer packed against the equivalent helix in an adjacent monomer related by pseudo-twofold symmetry.

A similar situation for a trigonal form of naphthalene 1,2-dioxygenase (NDO) has been described by Carredano *et al.* (2000). Their analysis of the structure-factor equation in such a case showed that the splitting of the *R*32 reflections into two pseudo-equivalent reflections sets in *R*3 results in differences in phases and not in their amplitudes and that the phase error from assuming the wrong space group is dependent on the parity of *l*. The magnitude of the difference is $4\pi l\Delta z$, where Δz is the separation between the two crystal patterns.

A plot of average amplitude as a function of *l* is shown in Fig. 3. The symmetrical nature of the plot reflects the equality of the amplitudes of the pseudo-equivalent reflections. The plot also shows the differences between the distribution of amplitudes for

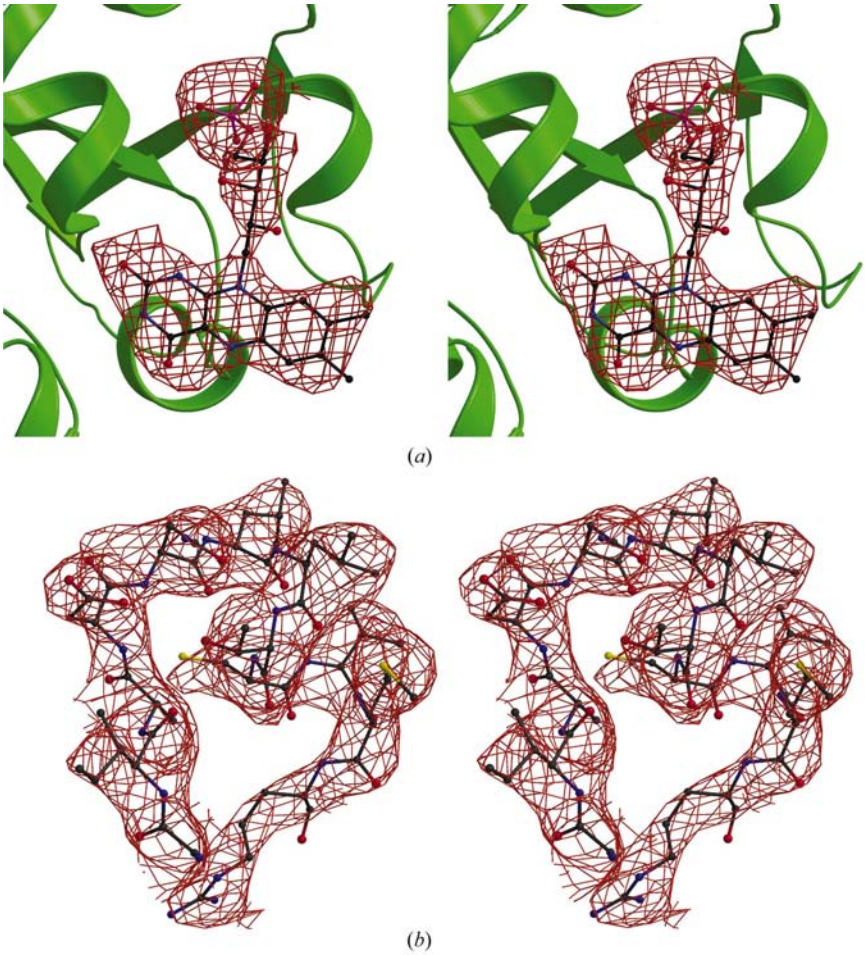

Figure 2
Stereoview showing electron density for PPC decarboxylase. (*a*) $F_o - F_c$ map contoured at 1.8σ showing the location of the bound FMN. The FMN molecule was not included in the refinement or in the calculated phases. (*b*) Section from a $2F_o - F_c$ composite omit map. The density corresponds to a helix–turn–helix region and is contoured at 1.0σ. This figure was created using *BOBSCRIPT* (Esnouf, 1999) and *Raster3D* (Merritt & Bacon, 1997).

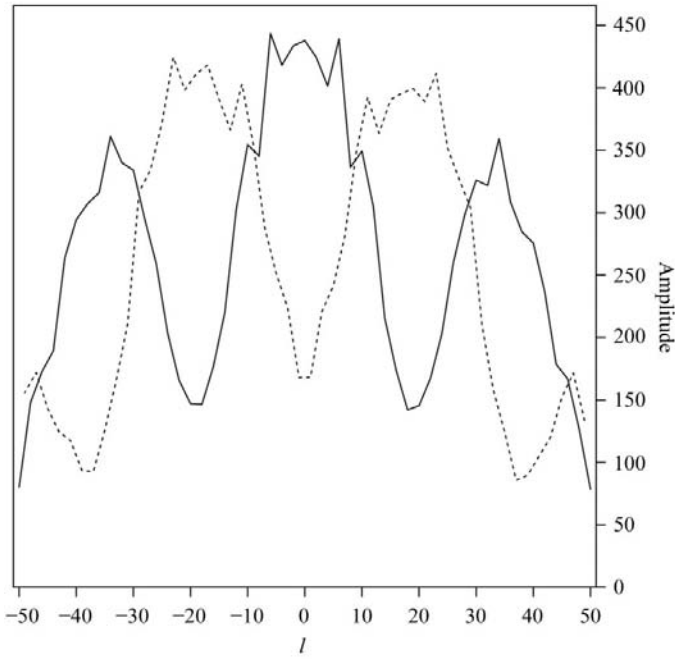

Figure 3
The distribution of average values of amplitude of reflections as a function of odd values of l (dashed line) and even values of l (full line).

odd and even values of l. This partition of the distributions is an expected consequence of the form of the modified structure-factor equations derived using geometrical considerations for space group $R32$. The crossover point between the two distributions represents a special situation in which the phase error is π, *i.e.* when

$$4\pi l \Delta z = \pi. \quad (1)$$

At this point on the reciprocal l axis, the amplitude and the phase error are the same for odd and even reflections (Carredano *et al.*, 2000) From the crystal structure, we know that Δz = 4.0/153.5 = 0.026 and solving for l in (1), the crossover occurs at about $l \simeq 10$.

The above analysis of data from the trigonal form of human PPC decarboxylase illustrates that unit-cell parameters can be misleading and that even $R_{\rm merge}$ does not always reveal the true space group. A plot of amplitudes as a function of a reciprocal value can be indicative of problems in space group arising from pseudo-translational symmetry as identified in PPC decarboxylase.

We thank Leslie Kinsland for assistance with preparation of the manuscript and figures. We thank Andrei Osterman and Matt Daugherty for providing us with their clone of the human *coaC*. We thank the NE-CAT beamline 8-BM of the Advanced Photon Source and the Cornell High Energy Synchrotron Source for provision of beam time.

References

Albert, A., Martinez-Ripoll, M., Espinosa-Ruiz, A., Yenush, L., Culianez-Macia, F. A. & Serrano, R. (2000). *Structure*, **8**, 961–969.
Begley, T. P., Kinsland, C. & Strauss, E. (2001). *Vitam. Horm.* **61**, 157–171.
Brünger, A. T., Adams, P. D., Clore, G. M., DeLano, W. L., Gros, P., Grosse-Kunstleve, R. W., Jiang, J.-S., Kuszewski, J., Nilges, M., Pannu, N. S., Read, R. J., Rice, L. M., Simonson, T. & Warren, G. L. (1998). *Acta Cryst.* D**54**, 905–921.
Carredano, E., Kauppi, B., Choudhury, D. & Ramaswamy, S. (2000). *Acta Cryst.* D**56**, 313–321.
Daugherty, M., Polanuyer, B., Farrell, M., Scholle, M., Lykidis, A., De Crecy-Lagard, V. & Osterman, A. (2002). *J. Biol. Chem.* **277**, 21431–21439.
Esnouf, R. M. (1999). *Acta Cryst.* D**55**, 938–940.
Hernandez-Acosta, P., Schmid, D. G., Jung, G., Culianez-Macia, F. A. & Kupke, T. (2002). *J. Biol. Chem.* **277**, 20490–20498.
Jones, T. A., Zou, J. Y., Cowan, S. W. & Kjeldgaard, M. (1991). *Acta Cryst.* A**47**, 110–119.
Kraulis, P. J. (1991). *J. Appl. Cryst.* **24**, 946–950.
Kupke, T. (2001). *J. Biol. Chem.* **276**, 27597–27604.
Kupke, T., Hernandez-Acosta, P., Steinbacher, S. & Culianez-Macia, F. A. (2001). *J. Biol. Chem.* **276**, 19190–19196.
Matthews, B. W. (1968). *J. Mol. Biol.* **33**, 491–497.
Merritt, E. A. & Bacon, D. J. (1997). *Methods Enzymol.* **277**, 505–524.
Navaza, J. & Saludjian, P. (1997). *Methods Enzymol.* **276**, 581–594.
Otwinowski, Z. & Minor, W. (1997). *Methods Enzymol.* **276**, 307–326.
Steinbacher, S., Hernandez-Acosta, P., Bieseler, B., Blaesse, M., Huber, R., Culianez-Macia, F. A. & Kupke, T. (2003). *J. Mol. Biol.* **327**, 193–202.
Strauss, E. & Begley, T. P. (2001). *J. Am. Chem. Soc.* **123**, 6449–6450.